NUMERICAL APPROXIMATION OF P-SYSTEMS WITH COULOMB FRICTIONAL DAMPING

KRISTY COFFEY* AND PIERRE A. GREMAUD†

Abstract. The asymptotic behavior of dissipative hyperbolic systems is very sensitive to the precise nature of the dissipation. Dry (Coulomb) friction is a limit case that has not been fully analyzed, for instance with respect to the asymptotic time behavior of solutions. Examples of such a problem are given by simple models of granular materials in containers. A numerical approach for generic problems of this type is proposed. The algorithm is based on the Discontinuous Galerkin method; the resulting scheme is briefly analyzed. Numerical results show the asymptotic stress profiles to be distinct but "close" to those predicted by an elementary analysis due to Janssen (1895) that still plays a role in Engineering today.

Key words. Coulomb friction, p-system, Discontinuous Galerkin, long time behavior

AMS subject classifications. 65M60, 74H40, 74S05, 35L50

1. Introduction.

This paper is concerned with a problem of the type

$$\partial_t u - \partial_z v = 0, \tag{1.1}$$

$$\partial_t v + \partial_z \sigma(u) \in h(u, v), \tag{1.2}$$

where σ and h are given functions of their arguments. In what follows, u will be thought of as a strain, v as a velocity and σ as a stress; Lagrangian coordinates are used throughout. The function σ satisfies $\sigma'(u) \leq 0$, making the above system hyperbolic. The function h typically corresponds to dissipative effects, in a sense to be made precise below.

If $h \equiv 0$, (1.1, 1.2) is the so-called p-system, a standard model problem. The case $h(u, v) = -\alpha v$, $\alpha \geq 0$ is also well studied [7, 13, 15, 19, 20, 26]. The popularity of that latter example is mainly explained by the relative ease with which energy arguments can be applied. Indeed, multiplying (1.2) by v clearly yields a right hand side with a definite sign. The diffusive character of more general cases requires a deeper analysis, see for instance [18] where h depends nonlinearly on v in a water-hammer problem. General approaches are starting to emerge, as in [12] where refined energy estimates are used.

In this paper, h is proportional to the stress σ. The resulting problem corresponds, for instance, to wave propagation in a granular material in the presence of dry – Coulomb– friction. A model is described in detail in Section 2. A discretization of the resulting problem by a Discontinuous Galerkin method is proposed in Section 3, together with an analysis of the semi-discretized problem. Numerical results are discussed in Section 4. In particular, the long time behavior of solutions to (1.1, 1.2) for specific initial/boundary conditions is studied numerically. Under the assumptions retained, and to the best of the authors' knowledge, the corresponding theoretical problem is open. This study also provides a dynamical version of the classical model of stress distribution proposed by Janssen in 1895 [16] described in Section 2.

*Department of Mathematics and Center for Research in Scientific Computation, North Carolina State University, Raleigh, NC 27695-8205, USA. Current address: Sandia National Laboratories, Albuquerque, NM.

†Department of Mathematics and Center for Research in Scientific Computation, North Carolina State University, Raleigh, NC 27695-8205, USA (gremaud@unity.ncsu.edu). Partially supported by the National Science Foundation (NSF) through grants DMS-0204578, DMS-0244488 and DMS-0410561.

2. Janssen's model. Consider a vertical container filled with granular material. When measuring the (average) stress in the material as a function of the depth d, one finds the stress to increase linearly with depth, for small values of d. However, at larger depths, the stress eventually asymptotes to a constant value, independent of d. This behavior results from the presence of frictional forces between the grains and the wall that partially support the material. More than a century ago, Janssen [16] proposed a mathematical model describing this phenomenon. Janssen's model, while far from perfect, provides approximate values for the stress variations in the material.

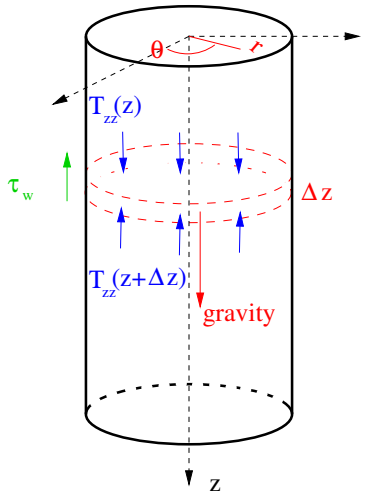

FIG. 2.1. Geometry and coordinates.

Janssen's model was originally written for right vertical cylindrical domains with circular cross sections. While more general geometries can easily be considered, see e.g. [6], we retain this simple setting and use the cylindrical coordinates (r, θ, z), see Figure 2.1. The mechanical state of the material is described by its stress tensor T and velocity v. Neglecting radial and angular dependencies, we get by virtue of axisymmetry (with a slight abuse of notation)

$$T(r,\theta,z) = \begin{bmatrix} T_{rr}(z) & 0 & T_{rz}(z) \\ 0 & T_{\theta\theta}(z) & 0 \\ T_{rz}(z) & 0 & T_{zz}(z) \end{bmatrix} \text{ and } v(r,\theta,z) = \begin{bmatrix} 0 \\ 0 \\ v(z) \end{bmatrix}.$$

Janssen's approach is based on three questionable assumptions

1. on each cross section, all physical quantities are constant;
2. T_{zz} and T_{rr} are principal, i.e., T is diagonal;
3. T_{zz} and T_{rr} are proportional: $k = \frac{T_{rr}}{T_{zz}}$ where k is determined experimentally.

The forces acting of a slice of material between z and $z + \Delta z$ are due to the internal stresses in the material: $\pi R^2(-T_{zz}(z+\Delta z) + T_{zz}(z))$, gravity: $\pi R^2 \Delta z \rho g$ and friction forces at the wall: $-2\pi R \Delta z \tau_w$, where R is the radius of the cylinder, ρ is the density, g is the acceleration due gravity and τ_w is the average wall shear stress. Therefore, conservation of momentum leads to

$$\rho\, \partial_t v + \partial_z T_{zz} + \frac{2}{R}\tau_w = \rho g.$$

We adopt the simple frictional model

$$\tau_w = \mu_w \operatorname{sgn}(v) T_{rr} = k\mu_w \operatorname{sgn}(v) T_{zz},$$

where μ_w is the coefficient of friction between wall and grains and sgn stands for the usual graph

$$\operatorname{sgn}(v) = \begin{cases} -1 & \text{if } v < 0, \\ (-1,1) & \text{if } v = 0, \\ 1 & \text{if } v > 0. \end{cases}$$

Note that sgn defined this way is a maximal monotone graph [4]. More involved frictional models can be found in the literature [21, 25]. Conservation of momentum can be rewritten

$$\rho\, \partial_t v + \partial_z \sigma - \rho g \in -\frac{1}{\lambda} \operatorname{sgn}(v)\sigma, \qquad z > 0, \tag{2.1}$$

where $\sigma = T_{zz}$ and $\lambda = \frac{R}{2k\mu_w}$ is a characteristic length. Constitutive assumptions are needed to close the model. Elastic responses are assumed from the granular medium. Accordingly, the stress σ is taken as a function of the strain u, more precisely

$$\sigma(u) = \max\{0, -\sigma_0 u |u|^{m-1}\}, \tag{2.2}$$

where $\sigma_0 > 0$ and $m >= 1$ are two constants, see [3] for derivation and range of validity. Relation (2.2) is compatible with both $\sigma \geq 0$, reflecting the fact that a granular material can support only compressive stresses, and $\sigma' \leq 0$ which corresponds to hyperbolicity.

Theoretical and experimental studies differ as to the values of m, respectively $m = 3/2$ [10] and $m = 2$ [9]. In [3], only the linear case $m = 1$ is studied. The material is supposed to be at rest before the experiments. The following values are typical [23]

$$R = 1/4\,\text{ft}, \quad k = 1/3, \quad \mu_w = \tan(\pi/9), \quad \rho g = 60\,\text{lb/ft}^3.$$

This determines the magnitude of the characteristic length λ as about $\lambda \approx 1$ft.

The problem can be rewritten in a non dimensional form by introducing

$$\bar{z} = \frac{z}{\lambda}, \bar{t} = \sqrt{\frac{\sigma_0}{\rho}}\,\frac{t}{\lambda}, \bar{v} = \frac{v}{\sqrt{\sigma_0/\rho}}, \bar{\sigma} = \frac{\sigma}{\sigma_0}.$$

From now on, we shall use exclusively the non dimensional quantities defined above; for convenience, the "bars" are omitted. The problem consists then in determining a velocity v and a strain u satisfying the following equations

$$\partial_t u - \partial_z v = 0, \qquad z > 0, t > 0, \tag{2.3}$$

$$\partial_t v + \partial_z \sigma(u) - G \in -\operatorname{sgn}(v)\sigma(u), \qquad z > 0, t > 0, \tag{2.4}$$

$$u(0,t) = u_b, \qquad \forall t > 0 \tag{2.5}$$

$$u(z,0) = v(z,0) = 0, \qquad \forall z > 0 \tag{2.6}$$

with $G = \frac{\rho g \lambda}{\sigma_0}$ and where u_b is such that $\sigma(u_b) \equiv \sigma_b$ corresponds to the normal stress applied at $z = 0$. Even though straightforward energy arguments along the lines

of [7, 13, 15, 19, 20, 26] cannot be applied, the above system admits the canonical entropy function $\mathcal{E}(u,v) = \frac{1}{2}v^2 + \Sigma(u)$ with $\Sigma'(u) = -\sigma(u)$; $\mathcal{E}$ is convex since $\sigma'(u) \leq 0$. Multiplying (2.3, 2.4) by $\mathcal{E}'$ and rearranging shows that every smooth solution satisfies

$$\partial_t \mathcal{E} + \partial_z \mathcal{F} = \mathcal{G},$$

where $\mathcal{F}(u,v) = v\sigma(u)$ is the entropy flux and $\mathcal{G}(u,v) = Gv - |v|\,\sigma(u)$. Recent progress has been made in the analysis of such systems. However, while (2.3, 2.4) can be shown to be entropy dissipative, it is not strictly entropy dissipative (see [12], Definition 2.2), precluding the direct application of the results from [12]. This difficulty is compounded by the possible presence of "vacuum states" (for nonlinear cases, $m > 1$, σ' vanishes for $u = 0$ and strict hyperbolicity is lost). Other difficulties include the presence of a boundary condition, (2.5), the stiffness of the source term, and the initial discontinuity at the boundary.

An outstanding question for partially dissipative hyperbolic systems is the asymptotic behavior of the solutions. This question has only recently been solved for the easier case of the p-system with frictional term proportional to the velocity, see [14, 15] and the references therein.

We take equilibrium solutions to be states for which the entropy production $\mathcal{G}$ vanishes [2]; hence, those solutions are here characterized by $v = 0$. Note that this is a different and more thermodynamical definition than the dynamical system approach taken in [12], which would require in the present case $\mathrm{sgn}(v) = 0$. While it seems natural to conjecture that the velocity converges to zero, $v(\cdot,t) \to 0$, as $t \to \infty$, the asymptotic behavior of the strain u is less clear. In his original work [16], Janssen considered that the material had reached a steady state. Further, it was assumed that the grains at rest were about to slide down (the slightest increase in vertical stress would result in motion). This corresponds to assuming $\mathrm{sgn}(v(\cdot,t)) \to 1$ as $t \to \infty$ in (2.4). As a consequence, the frictional force takes its largest allowable value. The resulting equations are

$$\partial_z \sigma + \sigma = G, \qquad z > 0, \tag{2.7}$$

$$\sigma(0) = \sigma_b, \tag{2.8}$$

where σ_b is the prescribed normal stress at $z = 0$. Equations (2.7, 2.8) is the model proposed by Janssen. It can easily be integrated and leads to the stress profile

$$\sigma(z) = (\sigma_b - G)e^{-z} + G. \tag{2.9}$$

In [3], (2.3–2.6) is proposed as a dynamical version of (2.7, 2.8). This new approach, while retaining some of the questionable assumptions from Janssen's model, provides a first description of how steady stress profiles are reached and of their nature. Boutreux et al. conclude from a partially analytical study that the stress predicted by Janssen was not reached. The present study expands on [3] in two directions: first, the role played by the elastic behavior of the material is examined in detail; second: the equations are numerically solved with a high order method (third order Discontinuous Galerkin method). Our numerical study shows that the asymptotic stress profiles are indeed different from, but close to, the profiles predicted by Janssen.

The gravitational effects being not of primarily interest, the cylinder is now set horizontally. The driving force is the boundary condition (2.8); in other words, $G = 0$ ($g = 0$) from now on, see Figure 2.2.

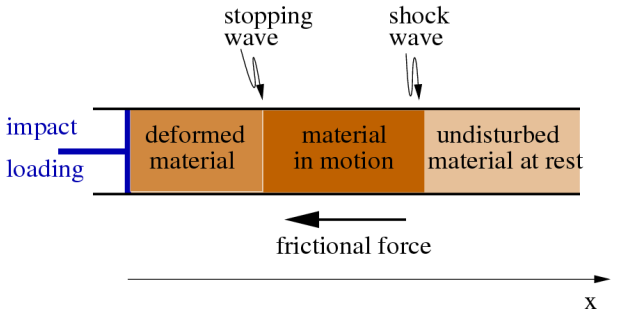

FIG. 2.2. Experimental setup: a semi infinite cylinder contains a compressible granular material; a pressure step is applied at the end.

As confirmed by the numerical experiments from Section 4, a stress front propagates through the material. The states to the right of the front being zero, a simple Rankine-Hugoniot analysis shows the front speed to be

$$s = |u_L|^{\frac{m-1}{2}}, \tag{2.10}$$

where u_L is the value of the strain at the front (from the left). In the linear case, $m = 1$, the speed of propagation is constant $s = 1$. The value v_L of the speed at the front (from the left) satisfies

$$v_L^2 = |u_L|^{m+1}. \tag{2.11}$$

In all cases, the amplitude of that pressure step is observed to decay due to the presence of the wall friction. A stopping wave is also formed behind the pressure front; behind this wave, all motion stops. As that latter wave propagates at a higher speed than the pressure step, the second front catches up with the first one. Therefore, due the dissipative frictional effects present in (2.3–2.6), the perturbation introduced at $z = 0$ only propagates a finite distance through the material before dying out. All motion eventually stops. Upper bounds for z and t are chosen accordingly, here L and T, respectively.

The precise behavior of the solutions is delicate. Consider for instance the situation to the left of the stopping front, where $v \equiv 0$. If we want to maintain $\partial_t v = 0$, then, from (2.2) and (2.4) (with $G = 0$), the term $\mathrm{sgn}(v)$ must satisfy

$$\mathrm{sgn}(v) = -m\,\frac{\partial_x u}{u}.$$

This is of course only possible if $|m\,\frac{\partial_x u}{u}| \leq 1$. As shown numerically in Section 4, there are cases for which the subsequent loading after passage of the stopping wave cannot be compensated by the frictional effects. We view this nonintuitive behavior as a sign of the possible shortcomings of the considered frictional model.

Some further analysis can be done in the linear case, i.e., $m = 1$ in (2.2). The resulting equations are

$$\partial_t u - \partial_z v = 0, \qquad z > 0, t > 0, \tag{2.12}$$

$$\partial_t v - \partial_z u \in \mathrm{sgn}(v)u, \qquad z > 0, t > 0, \tag{2.13}$$

with again (2.5, 2.6) as boundary and initial conditions. For small times, i.e., before formation of the stopping wave, the above problem can be solved analytically. More

precisely, consider (2.12, 2.13) in the domain where $v > 0$. The equation can be rewritten

$$\partial_{tt} u - \partial_{zz} u - \partial_z u = 0. \tag{2.14}$$

In the domain where $v > 0$, a standard Fourier transform method leads to [3]

$$u(z,t) = \begin{cases} u_b e^{-z/2} \left(\cosh(\frac{t-z}{2}) - \frac{t}{2} \int_{z/t}^{1} \cosh(\frac{yt-z}{2}) \frac{J_1((t/2)\sqrt{1-y^2})}{\sqrt{1-y^2}}\, dy \right) & \\ \qquad \text{if } z \le t, & \\ 0 \qquad \text{if } z > t, & \end{cases}$$

where J_1 is the Bessel function of the first kind of order 1. The value of u at the front of the pressure wave is thus at time t: $u(t,t) = u_b e^{-t/2}$, and consequently the value of the velocity on that front is $v(t,t) = -u_b e^{-t/2}$. The velocity itself v can be obtained by integrating (2.12)

$$v(z,t) = \begin{cases} -u_b e^{-t/2} - \int_z^t \partial_t u \, dy & \text{if } z \le t, \\ 0 & \text{otherwise.} \end{cases}$$

Note that for a given z, the above expression for the velocity eventually becomes negative as t increases, whereas the above solution is only valid where the velocity is positive. A physically based modification of the approach, as opposed to mathematically based, is proposed in [3].

3. Numerical method. Equations (2.3, 2.4) are discretized in space using a Discontinuous Galerkin (DG) method of order 3 see [5] and the references therein. For $N > 0$, we set $\Delta z = L/N$ and consider a uniform partition of $(0, L)$ as $\{z_{j+1/2}\}_{j=0}^{N}$, where $z_{j+1/2} = j\Delta z$. This defines N intervals $I_j = (z_{j-1/2}, z_{j+1/2})$ of center $z_j = (j - 1/2)\Delta z$, $j = 1, \ldots, N$. At any given time, the numerical solutions are sought in the space

$$V_h = \{w \in L^1(0, L) : v|_{I_j} \in P^2(I_j), j = 1, \ldots, N\},$$

where $P^2(I)$ stands for the space of degree 2 polynomials on I. More precisely, for $t \in (0, T)$ both of the two unknowns u and v are approximated by piecewise polynomial functions of degree 2 denoted u_h and v_h respectively, where

$$u_h|I_j = \sum_{l=0}^{2} u_j^l(t) \Phi_j^l(z), \qquad v_h|I_j = \sum_{l=0}^{2} v_j^l(t) \Phi_j^l(z),$$

where $\{u_j^l\}$ and $\{v_j^l\}$ are coefficients to be determined and $\Phi_j^l(z) = P_l(\frac{2(z-z_j)}{\Delta z})$, $l = 0, 1, 2$, P_l being the l-th Legendre polynomial on the interval $(-1, 1)$. The unknowns u_h and v_h satisfy the relations

$$\int_{I_j} (\partial_t u_h p - v_h\, \partial_z p)\, dx + \mathcal{F}(v_h)(z_{j+\frac{1}{2}}) p(z^-_{j+\frac{1}{2}}) - \mathcal{F}(v_h)(z_{j-\frac{1}{2}}) p(z^+_{j-\frac{1}{2}}) = 0, \tag{3.1}$$

$$\int_{I_j} (\partial_t v_h q - \sigma(u_h)\, \partial_z q)\, dx + \mathcal{G}(u_h)(z_{j+\frac{1}{2}}) q(z^-_{j+\frac{1}{2}}) - \mathcal{G}(u_h)(z_{j-\frac{1}{2}}) q(z^+_{j-\frac{1}{2}}) \in -\int_{I_j} \mathrm{sgn}(v_j^0)\, \sigma(u_h) q \, dx, \tag{3.2}$$

for any $t > 0$, for any $j = 1, \dots, N$, for any p, $q \in V_h$. In (3.1, 3.2), $\mathcal{F}$ and $\mathcal{G}$ are the local Lax Friedrichs numerical fluxes consistent with the fluxes in (2.3, 2.4). Note that the argument of sgn has been reduced to the cell average of the velocity v_j^0; how to deal precisely with $\mathrm{sgn}(v_j^0)$ will be described below. In agreement with the initial conditions (2.6), we set $u_h(\cdot, 0) = v_h(\cdot, 0) = 0$. The boundary condition (2.5) is enforced through the numerical flux, see [5] for details.

Grouping all the unknowns from the latter system into the function

$$\begin{aligned} U_h : [0,T] &\to \mathrm{R}^{6N} \\ t &\mapsto U_h(t) = [u_1^0(t), u_1^1(t), u_1^2(t), v_1^0(t), v_1^1(t), v_1^2(t), \dots, v_N^2(t)], \end{aligned}$$

the semi-discretized problem in space can be rewritten

$$\frac{dU_h}{dt} + R_h(U_h) \ni L_h(U_h), \qquad t > 0, \tag{3.3}$$

$$U_h(0) = U_0, \tag{3.4}$$

where L_h results from the discretization of the divergence part of the original system while R_h corresponds to the nonlinear friction term. More precisely,

$$\begin{aligned} L_h : \mathrm{R}^{6N} &\to \mathrm{R}^{6N} \\ U_h &\mapsto L_h(U_h) = [\dots, \mathcal{L}_j^0, \mathcal{L}_j^1, \mathcal{L}_j^2, \mathcal{N}_j^0, \mathcal{N}_j^1, \mathcal{N}_j^2, \dots], \end{aligned}$$

where $\mathcal{L}_j^l$, $l = 0, 1, 2$, $j = 1, \dots, N$, are linear functions of v_{j-1}^0, v_{j-1}^1, v_{j-1}^2, v_j^0, v_j^1, v_j^2, v_{j+1}^0, v_{j+1}^1, v_{j+1}^2, while $\mathcal{N}_j^l$, $l = 0, 1, 2$, $j = 1, \dots, N$, have the same nature as the function σ, see (2.2), i.e., they are polynomials of degree m in u_{j-1}^0, u_{j-1}^1, u_{j-1}^2, u_j^0, u_j^1, u_j^2, u_{j+1}^0, u_{j+1}^1, u_{j+1}^2. Further,

$$\begin{aligned} R_h : \mathrm{R}^{6N} &\to \mathrm{R}^{6N} \\ U_h &\mapsto R_h(U_h) = [0, 0, 0, \mathrm{sgn}(v_1^0)\mathcal{R}_1^0, \mathrm{sgn}(v_1^0)\mathcal{R}_1^1, \mathrm{sgn}(v_1^0)\mathcal{R}_1^2, \dots, \\ &\qquad 0, 0, 0, \mathrm{sgn}(v_j^0)\mathcal{R}_j^0, \mathrm{sgn}(v_j^0)\mathcal{R}_j^1, \mathrm{sgn}(v_j^0)\mathcal{R}_j^2, \dots], \end{aligned}$$

where $\mathcal{R}_j^l$ is a polynomial of degree m in u_j^0, u_j^1, u_j^2, $l = 0, 1, 2$, $j = 1, \dots, N$.

If the elastic constitutive law (2.2) is replaced by an Lipschitz regularized law, i.e.,

$$\sigma^\star(u) = \begin{cases} \sigma(u) & \text{if } |\, u \,| \le u^\star, \\ \sigma'(u^\star)(u - u^\star) + \sigma(u^\star) & \text{if } |\, u \,| > u^\star, \end{cases} \tag{3.5}$$

where $u^\star$ is chosen large enough, then it can be shown that the semi-discretized problem (3.3,3.4) has a unique solution.

LEMMA 3.1. *If σ is replaced by $\sigma^\star$, then there exists $\omega > 0$ such that $A_h = R_h - L_h + \omega I$ is a maximal monotone operator on R^{6N}.*

Proof. Let $\vec{u}_j = [u_j^0, u_j^1, u_j^2]^T$ and $\vec{v}_j = [v_j^0, v_j^1, v_j^2]^T$. The operator $A_h : \mathrm{R}^{6N} \to \mathrm{R}^{6N}$ takes the form

$$A_h : U_h = \begin{bmatrix} \dots \\ \vec{u}_j \\ \vec{v}_j \\ \dots \end{bmatrix} \mapsto \begin{bmatrix} \dots \\ 0 \\ 0 \\ 0 \\ \mathrm{sgn}(v_j^0)\mathcal{R}_j^0(\vec{u}_j) \\ \mathrm{sgn}(v_j^0)\mathcal{R}_j^1(\vec{u}_j) \\ \mathrm{sgn}(v_j^0)\mathcal{R}_j^2(\vec{u}_j) \\ \dots \end{bmatrix} - \begin{bmatrix} \dots \\ \mathcal{L}_j^0(\vec{v}_{j-1}, \vec{v}_j, \vec{v}_{j+1}) \\ \mathcal{L}_j^1(\vec{v}_{j-1}, \vec{v}_j, \vec{v}_{j+1}) \\ \mathcal{L}_j^2(\vec{v}_{j-1}, \vec{v}_j, \vec{v}_{j+1}) \\ \mathcal{N}_j^0(\vec{u}_{j-1}, \vec{u}_j, \vec{u}_{j+1}) \\ \mathcal{N}_j^1(\vec{u}_{j-1}, \vec{u}_j, \vec{u}_{j+1}) \\ \mathcal{N}_j^2(\vec{u}_{j-1}, \vec{u}_j, \vec{u}_{j+1}) \\ \dots \end{bmatrix} + \omega \begin{bmatrix} \dots \\ \vec{u}_j \\ \vec{v}_j \\ \dots \end{bmatrix}.$$

We have

$$
\begin{aligned}
(A_h(U_h) - A_h(\bar U_h), U_h - \bar U_h) = \dots \\
&\left(-\mathcal{L}_j^0(\vec v_{j-1}, \vec v_j, \vec v_{j+1}) + \mathcal{L}_j^0(\bar{\vec v}_{j-1}, \bar{\vec v}_j, \bar{\vec v}_{j+1})\right)(u_j^0 - \bar u_j^0) \\
&+ \left(-\mathcal{L}_j^1(\vec v_{j-1}, \vec v_j, \vec v_{j+1}) + \mathcal{L}_j^1(\bar{\vec v}_{j-1}, \bar{\vec v}_j, \bar{\vec v}_{j+1})\right)(u_j^1 - \bar u_j^1) \\
&+ \left(-\mathcal{L}_j^2(\vec v_{j-1}, \vec v_j, \vec v_{j+1}) + \mathcal{L}_j^2(\bar{\vec v}_{j-1}, \bar{\vec v}_j, \bar{\vec v}_{j+1})\right)(u_j^2 - \bar u_j^2) \\
&+ \left(-\mathcal{N}_j^0(\vec u_{j-1}, \vec u_j, \vec u_{j+1}) + \mathcal{N}_j^0(\bar{\vec u}_{j-1}, \bar{\vec u}_j, \bar{\vec u}_{j+1})\right)(v_j^0 - \bar v_j^0) \\
&+ \left(-\mathcal{N}_j^1(\vec u_{j-1}, \vec u_j, \vec u_{j+1}) + \mathcal{N}_j^1(\bar{\vec u}_{j-1}, \bar{\vec u}_j, \bar{\vec u}_{j+1})\right)(v_j^1 - \bar v_j^1) \\
&+ \left(-\mathcal{N}_j^2(\vec u_{j-1}, \vec u_j, \vec u_{j+1}) + \mathcal{N}_j^2(\bar{\vec u}_{j-1}, \bar{\vec u}_j, \bar{\vec u}_{j+1})\right)(v_j^2 - \bar v_j^2) \\
&+ \left(\mathrm{sgn}(v_j^0)\mathcal{R}_j^0(\vec u_j) - \mathrm{sgn}(\bar v_j^0)\mathcal{R}_j^0(\bar{\vec u}_j)\right)(v_j^0 - \bar v_j^0) \\
&+ \left(\mathrm{sgn}(v_j^0)\mathcal{R}_j^1(\vec u_j) - \mathrm{sgn}(\bar v_j^0)\mathcal{R}_j^1(\bar{\vec u}_j)\right)(v_j^1 - \bar v_j^1) \\
&+ \left(\mathrm{sgn}(v_j^0)\mathcal{R}_j^2(\vec u_j) - \mathrm{sgn}(\bar v_j^0)\mathcal{R}_j^2(\bar{\vec u}_j)\right)(v_j^2 - \bar v_j^2) \\
&+ \omega\left(\dots + (u_j^0 - \bar u_j^0)^2 + (u_j^1 - \bar u_j^1)^2 + (u_j^2 - \bar u_j^2)^2 + \dots\right. \\
&\qquad \left. \dots + (v_j^0 - \bar v_j^0)^2 + (v_j^1 - \bar v_j^1)^2 + (v_j^2 - \bar v_j^2)^2 + \dots\right).
\end{aligned}
$$

The first six lines can be estimated by repeated Cauchy-Schwartz inequalities to yield

$$
\begin{aligned}
(A_h(U_h) - A_h(\bar U_h), U_h - \bar U_h) \geq \dots \\
&+ (\omega - L)\left(\dots + (u_j^0 - \bar u_j^0)^2 + (u_j^1 - \bar u_j^1)^2 + (u_j^2 - \bar u_j^2)^2 + \dots\right. \\
&\qquad \left. \dots + (v_j^0 - \bar v_j^0)^2 + (v_j^1 - \bar v_j^1)^2 + (v_j^2 - \bar v_j^2)^2 + \dots\right) \\
&+ \dots \\
&+ \left(\mathrm{sgn}(v_j^0)\mathcal{R}_j^0(\vec u_j) - \mathrm{sgn}(\bar v_j^0)\mathcal{R}_j^0(\bar{\vec u}_j)\right)(v_j^0 - \bar v_j^0) \\
&+ \left(\mathrm{sgn}(v_j^0)\mathcal{R}_j^1(\vec u_j) - \mathrm{sgn}(\bar v_j^0)\mathcal{R}_j^1(\bar{\vec u}_j)\right)(v_j^1 - \bar v_j^1) \\
&+ \left(\mathrm{sgn}(v_j^0)\mathcal{R}_j^2(\vec u_j) - \mathrm{sgn}(\bar v_j^0)\mathcal{R}_j^2(\bar{\vec u}_j)\right)(v_j^2 - \bar v_j^2) + \dots,
\end{aligned}
$$

where $L > 0$ depends on the Lipschitz constants of $\mathcal{L}_j^l$ and $\mathcal{N}_j^l$, $l = 0, 1, 2$, $j = 1, \dots, N$, i.e., on $\sigma'(u^\star)$, by consistency of the numerical fluxes. Since $\sigma \geq 0$, see (2.2), we have for each of the last three terms, by monotonicity of sgn

$$
\begin{aligned}
\left(\mathrm{sgn}(v_j^0)\mathcal{R}_j^l(\vec u_j) \right. &- \left. \mathrm{sgn}(\bar v_j^0)\mathcal{R}_j^l(\bar{\vec u}_j)\right)(v_j^l - \bar v_j^l) \\
&= \mathcal{R}_j^l(\vec u_j)\left(\mathrm{sgn}(v_j^0) - \mathrm{sgn}(\bar v_j^0)\right)(v_j^l - \bar v_j^l) \\
&+ \mathrm{sgn}(\bar v_j^0)\left(\mathcal{R}_j^l(\vec u_j) - \mathcal{R}_j^l(\bar{\vec u}_j)\right)(v_j^l - \bar v_j^l) \\
&\geq 0 - L'\left((u_j^0 - \bar u_j^0)^2 + (u_j^1 - \bar u_j^1)^2 + (u_j^2 - \bar u_j^2)^2 + (v_j^l - \bar v_j^l)^2\right),
\end{aligned}
$$

where L' depends on $\sigma'(u^\star)$. Putting the last two inequalities together, it is now clear that ω can be chosen, independently of N, such that $(A_h(U_h) - A_h(\bar U_h), U_h - \bar U_h) \geq 0$, establishing the monotonicity of A_h. Its maximality in the set of monotone operators results from the maximality of sgn. ∎

For any $X \in \mathrm{R}^{6N}$, the non empty set $A_h(X)$ is then closed and convex in R^{6N}; its element of minimum norm, the minimal selection of $A_h(X)$ is denoted by $A_h(X)^o$. The next result follows directly from classical results, see for instance [4], Chapitre III.

THEOREM 3.2. *If σ is replaced by $\sigma^\star$, then there exists a unique strong solution U_h to the semi-discretized problem (3.3, 3.4). Further, U_h is Lipschitz continuous and*

its right derivative $\frac{d^+U_h}{dt}$ *exists for every* t *and coincides with the minimal selection of* $-A_h(U_h)$*, i.e.*

$$\frac{d^+U_h}{dt} + A_h(U_h)^o = 0, \qquad \text{for any } t \geq 0.$$

The above problem has to be fully discretized. While explicit time discretization methods are the natural choice for hyperbolic problems, those algorithms are well known to perform poorly on differential inclusions and stiff ODEs [8]. While the previous theorem leads to a natural time discretization of the inclusion, see below, a standard explicit time discretization is retained for the hyperbolic part. The time interval $(0,T)$ is partitioned in N_t uniform intervals (t^n, t^{n+1}) where $t^n = n\Delta t$, $n = 0, \ldots, N_t - 1$ and $\Delta t = \frac{T}{N_t}$.

To go from $U_h^n \approx U_h(t^n)$ to $U_h^{n+1} \approx U_h(t^{n+1})$

(i) set $U_h^{(0)} = U_h^n$,

(ii) $U_h^{(1)} = \Lambda\Pi_h \left\{ U_h^{(0)} + \Delta t L_h(U_h^{(0)}) - \Delta t\, R_h^{(1)} \right\}$,

(iii) $U_h^{(2)} = \Lambda\Pi_h \left\{ \frac{3}{4}U_h^{(0)} + \frac{1}{4}U_h^{(1)} + \frac{\Delta t}{4} L_h(U_h^{(1)}) - \frac{\Delta t}{2}\, R_h^{(2)} \right\}$,

(iv) $U_h^{(3)} = \Lambda\Pi_h \left\{ \frac{1}{3}U_h^{(0)} + \frac{2}{3}U_h^{(2)} + \frac{2\Delta t}{3} L_h(U^{(2)}) - \Delta t\, R_h^{(3)} \right\}$,

(v) $U_h^{n+1} = U_h^{(3)}$,

where $\Lambda\Pi_h$ is a modified van Leer slope limiter [22]. The explicit part of the algorithm is the third order TVD Runge-Kutta method originally proposed in [24]. In the absence of a right hand side, the stage variables $U_h^{(i)}$, $i = 1, 2, 3$, have respective stage orders 1, 1 and 3 and correspond to approximations at time t^{n+1}, $t^n + \frac{\Delta t}{2}$ and t^{n+1} respectively. The inclusion is solved at those respective times for each of the three stages, before slope limiting is applied. More precisely, considering the first stage as an illustration, $R_h^{(1)}$ is computed as follows.

1. As the strain equation does not have a right side, the strain is updated from the explicit TVD Runge-Kutta method.
2. The new velocity in $U_h^{(1)}$ is *assumed* equal to zero and, for the velocity equations, $R_h^{(1)}$ is computed so as to satisfy (ii), i.e., $U_h^{(0)} + \Delta t L_h(U_h^{(0)}) - \Delta t\, R_h^{(1)} = 0$.
3. The value of $\mathrm{sgn}(v_j^0)$ is computed from $R_h^{(1)}$. If $\mathrm{sgn}(v_j^0) > 1$, then we set $\mathrm{sgn}(v_j^0) = 1$ and solve (ii) for the new velocity in cell j. If $\mathrm{sgn}(v_j^0) < -1$, then we set $\mathrm{sgn}(v_j^0) = -1$ and solve (ii) for the new velocity in cell j.
4. The slope limiter is applied.

When possible, it may be advantageous to design numerical schemes that preserve equilibrium solutions of the problem under consideration, see for instance [1, 11] and the literature on well balanced schemes. Here equilibrium solutions satisfy $v_\infty \equiv 0$ and

$$\begin{aligned} \partial_z \sigma(u_\infty) &= -s(z)\, \sigma(u_\infty), \qquad z > 0 \\ u_\infty(0) &= u_b, \end{aligned}$$

for *any* function s taking its values in $[-1, 1]$. The corresponding plethora of solutions makes this approach problematic. Instead, a weaker a posteriori check is performed, see comparison with the solution to (4.1, 4.2) performed in Section 4.

4. Numerical results. In the following experiments, the system (2.3-2.6) is solved with $G = 0$ and the boundary condition $u(0,t) = u_b = -1$, $t > 0$. Unless otherwise stated, 400 spatial cells are used. The time step is determined through the experimental stability condition

$$c\frac{\Delta t}{\Delta x} \leq \frac{1}{5},$$

where $c = \sqrt{-\sigma'(u^\star)}$, $u^\star$ being as in Section 3 an approximate value for the largest observed strain, see [5].

Numerical results corresponding to the three different elasticity models considered in Section 2 are presented: $m = 1$ [3], $m = 3/2$ [10] and $m = 2$ [9]. The calculations are stopped once the strain has settled to its asymptotic value.

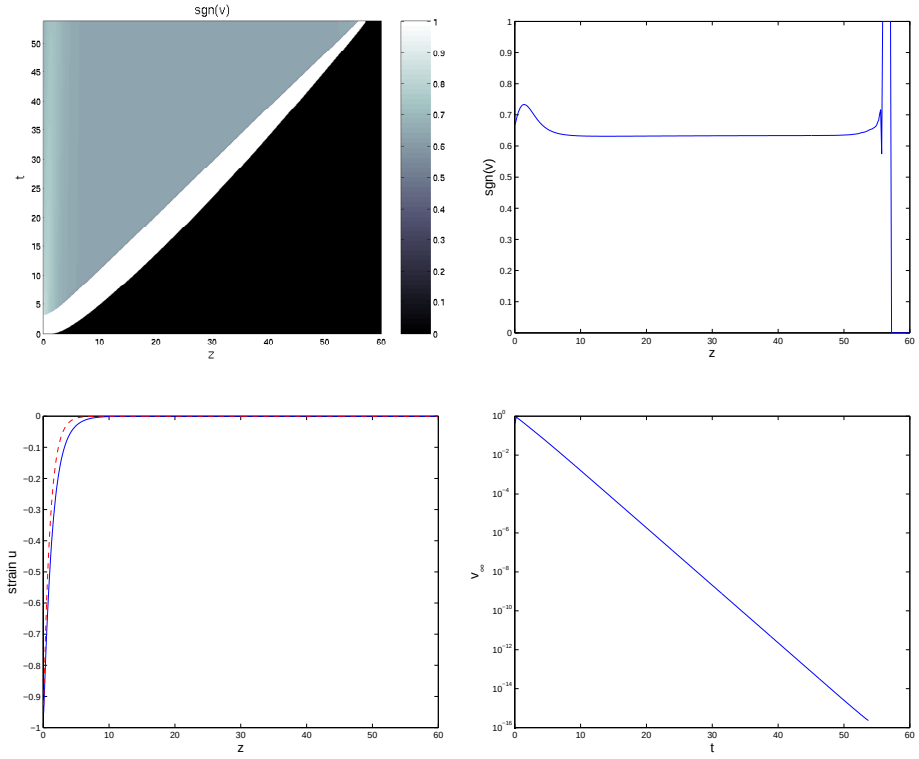

FIG. 4.1. Case $m = 1$. Top left: sgn(v); top right: asymptotic profile of sgn(v); bottom left: asymptotic strain (solid line) and Janssen's solution (dashed line); bottom right: log plot of $v_\infty(t) = \max_{z>0} v(z,t)$.

Figure 4.1, top left, shows the behavior of sgn(v). In the black area (sgn(v) = 0), the material is at rest and has not been disturbed by the perturbation introduced at the left boundary. Motion takes place in the white area (sgn(v) = 1). The asymptotic profiles of both sgn(v) and strain are displayed in Figure 4.1, top right and bottom left respectively. The asymptotic strain is clearly different from the solution predicted through Janssen's analysis. Figure 4.1, bottom right, illustrates the asymptotic decay of the maximum velocity $v_\infty(t) = \max_{z>0} v(z,t)$ as t increases.

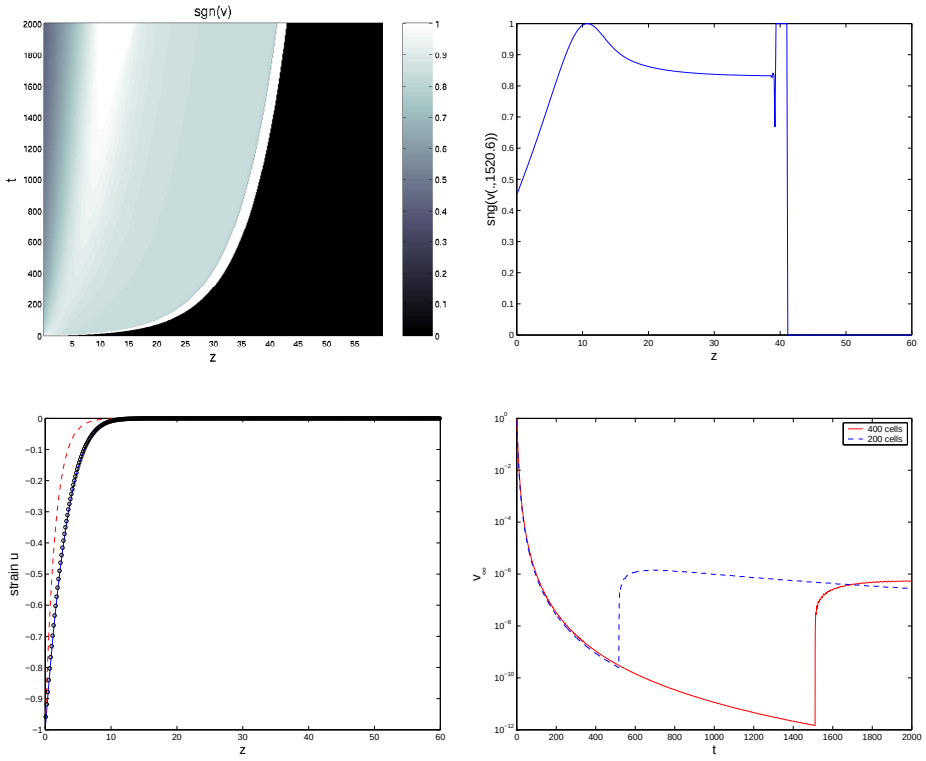

FIG. 4.2. Case $m = 3/2$. Top left: $\mathrm{sgn}(v)$; top right: $\mathrm{sgn}(v)$ at the time corresponding to critical loading, i.e., $\mathrm{sgn}(v(\cdot, t \approx 1520))$; bottom left: asymptotic strain (solid line), Janssen's solution (dashed line) and and approximate stationary strain $u_{h,\infty}$ computed from the asymptotic values of $\mathrm{sgn}(v)$ (circles); bottom right: log plot of $v_\infty(t) = \max_{z>0} v(z,t)$; dashed line: 200 spatial cells, solid line: 400 spatial cells .

The case $m = 3/2$ is substantially different from the linear case $m = 1$. First, the speed of propagation is not constant but decreases as the strain decreases in absolute value. This behavior is clear from Figure 4.2, top left, which illustrates the behavior of $\mathrm{sgn}(v)$. A "loading wave" is observed on the left of the domain. Our calculations show that loading is strong enough to reach the critical value $\mathrm{sgn}(v) = 1$. In Figure 4.2, top right, $\mathrm{sgn}(v)$ is displayed at the time corresponding to critical loading, here, $t \approx 1520$ (for a mesh with 400 cells). After that time, unloading ensues; subsequent damping and convergence to zero are extremely slow. Figure 4.2, bottom right, illustrates the onset of this phenomenon. The precise behavior of the velocity in that regime, unlike that of the strain, is sensitive to the discretization parameters. The sensitivity on the mesh size is displayed on that figure. No significant changes in the strain u can be numerically observed during the subsequent slow transition to equilibrium. This claim can be supported by numerically solving

$$\partial_z \sigma(u_{h,\infty}(z_j)) = -s(z_j)\, \sigma(u_{h,\infty}(z_j)), \qquad j = 1, \ldots, N \tag{4.1}$$

$$u_{h,\infty}(0) = u_b, \tag{4.2}$$

for $u_{h,\infty}$, where $s(z_j) = \mathrm{sgn}(v_j^0)$ at the end of the computational time interval. This problem corresponds to one of our two main equations, (2.4), with the time derivative

term dropped and sgn(v) set equal to the corresponding asymptotic numerical values. The results are displayed in Figure 4.2, bottom left. Again, the asymptotic strain is clearly different from Janssen's. Further, comparison of the asymptotic strain profile with $u_{h,\infty}$ shows very good agreement.

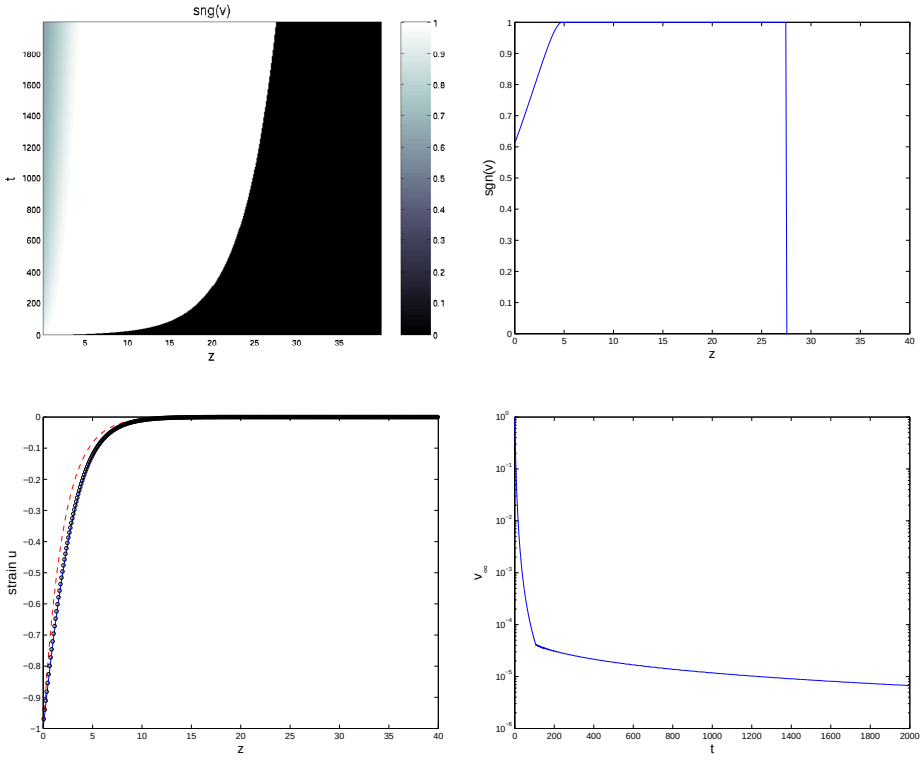

FIG. 4.3. Case $m = 2$. Top left: sgn(v); top right: asymptotic profile of sgn(v); bottom left: asymptotic strain (solid line), Janssen's solution (dashed line) and and approximate stationary strain $u_{h,\infty}$ computed from the asymptotic values of sgn(v) (circles); bottom right: log plot of $v_\infty(t) = \max_{z>0} v(z,t)$ (400 spatial cells) .

The case $m = 2$ is somewhat similar to $m = 3/2$. However, unlike the previous case, most of the material stays loaded sgn(v) $= 1$ after the passage of the pressure wave, as can be seen from the behavior of sgn(v) in Figure 4.3, top left. The stopping wave which corresponds to the left boundary of the domain in which sgn(v) $= 1$ moves here very slowly, as can be seem from Figure 4.3, top right. The maximum velocity also decreases much more slowly than in the previous case, see Figure 4.3, bottom right. The asymptotic behavior of the strain is displayed in Figure 4.3, bottom left. Again, the numerical strain obtained at the end of the computational time interval is compared with both Janssen's solution and the solution to the auxiliary problem (4.1,4.2) with $m = 2$. As more of the material stays fully loaded, it is not surprising to observe from Figure 4.3, bottom left, that the asymptotic strain, while clearly distinct from Janssen's, is closer to it than it was for $m = 3/2$.

REFERENCES

[1] E. Audusse, F. Bouchut, M.-O. Bristeau, R. Klein and B. Perthame, *A fast and stable well-balanced scheme with hydrostatic reconstruction for shallow water flows*, SIAM J. Sci. Comput., 25 (2004), pp. 2050–2065.

[2] G. Boillat and T. Ruggeri, *On the shock structure problem for hyperbolic balance laws and convex entropy*, Contin. Mech. Thermodyn., 10 (1998), pp. 285–292.

[3] T. Boutreux, E. Raphaël and P.G. de Gennes, *Propagation of a pressure step in a granular material: the role of wall friction*, Physical Rev. E, 55 (1997), pp. 5759–5773.

[4] H. Brezis, *Opérateurs maximaux monotones et semi-groupes de contractions dans les espaces de Hilbert*, North-Holland, Mathematical Studies, #50, (1973).

[5] B. Cockburn, S.Y. Lin and C.W. Shu, *TVB Runge-Kutta local projection discontinuous Galerkin finite element method for conservation laws III: one dimensional systems*, J. Comput. Phys., 84 (1989), pp. 90–113.

[6] K.A. Coffey and P.A. Gremaud, *Numerical simulation of aerated powder consolidation*, Int. J. Nonlinear Mech., 38 (2003), pp. 1185–1194.

[7] C.M. Dafermos, *A System of Hyperbolic Conservation Laws with Frictional Damping*, Z. angew. Math. Phys., 46 (1995), pp. S294–S307.

[8] A. Dontchev and F. Lempio, *Difference methods for differential inclusions: a survey*, SIAM Review, 34 (1992), pp. 263–294.

[9] J. Duffy and R.D. Mindlin, *Stress-strain relations and vibrations of a granular medium*, J. Appl. Mech. (AMSE), 24 (1957), pp.585–593.

[10] J.D. Goddard, *Nonlinear elasticity and pressure-dependent wave speeds in granular media*, Proc. R. Soc. Lond. A, 430 (1990), pp. 105–131.

[11] J.M. Greenberg and A.Y. Leroux *A well-balanced scheme for the numerical processing of source terms in hyperbolic equations*, SIAM J. Numer. Anal., 33 (1996), pp.1–16.

[12] B. Hanouzet and R. Natalini, *Global existence of smooth solutions for partially dissipative hyperbolic systems with a convex entropy*, Arch. Ration. Mech. Anal., 169 (2003), pp. 89–117.

[13] Ling Hsiao and Tai-Ping Lui, *Convergence to Nonlinear Diffusion Waves for Solutions of a System of Hyperbolic Conservation Laws with Damping*, Commun. Math. Phys., 143 (1992), pp 599-605.

[14] Feimin Huang, P. Marcati and Ronghua Pan, *Convergence to Barenblatt solution for the compressible Euler equations with damping and vacuum*, Preprint, Department of Mathematics, Georgia Tech, 2002.

[15] Feimin Huang and Ronghua Pan, *Convergence rate for compressible Euler equations with damping and vacuum*, Arch. Ration. Mech. Anal., 166 (2003), pp. 359–376.

[16] H.A. Janssen, *Versuche über Getreidedruck in Silozellen*, Zeitschrift des Vereines Deutscher Ingenieure, 39 (1895), pp. 1045–1049.

[17] C.T. Kelley, *Iterative methods for linear and nonlinear equations*, Frontiers of Applied Mathematics, #16, SIAM (1995).

[18] M.B. Luskin and B. Temple, *The existence of a global weak solution to the non-linear water-hammer problem*, Comm. Pure Appl. Math., 35 (1982), pp. 697–735.

[19] P. Marcati, Ming Mei, *Convergence to nonlinear diffusion waves for solutions of the initial boundary problem to the hyperbolic conservation laws with damping*, Quart. Appl. Math. 58 (2000), pp. 763–784.

[20] K. Nishihara, W. Wang and T. Yang, *L_p-convergence rate to nonlinear diffusion waves for p-system with damping*, J. Differential Eqs, 161 (2000), pp. 191–218.

[21] J.T. Oden, J.A.C. Martins, *Models and computational methods for dynamic friction phenomena*, Comp. Meth. Appl. Mech. Eng., 52 (1985), pp. 527–634.

[22] S. Osher, *Convergence of generalized MUSCL schemes*, SIAM J. Numer. Anal., 22 (1984), pp. 947–961.

[23] A.T. Royal, *Private communication*, Jenike & Johanson, inc., 2003.

[24] C.W. Shu, *TVD time discretizations*, SIAM J. Sci. Stat. Comput., 9 (1988), pp. 1073–1084.

[25] D.E. Stewart, *Rigid-body dynamics with friction and impact*, SIAM Review, 42 (2000), pp. 3–39.

[26] Huijiang Zhao, *Convergence to strong nonlinear diffusion waves for solutions of p-system with damping*, J. Differential Eqs., 174 (2001), pp. 200–236.